Astron. Astrophys. 364, 829–834 (2000)

ASTRONOMY AND ASTROPHYSICS

Small-scale flow field in a sunspot penumbra

W. Schmidt and R. Schlichenmaier

Kiepenheuer-Institut für Sonnenphysik, Schöneckstrasse 6, 79104 Freiburg, Germany (wolfgang,schliche @kis.uni-freiburg.de)

Received 15 May 2000 / Accepted 1 September 2000

Abstract. We have measured velocity maps of a round sunspot near the center of the solar disk. We derive the small-scale velocity field of the penumbra in the deep photosphere. Superimposed on a radial outflow, we find up– and downflows, which are associated with bright and dark features: The flow in the dark component of the penumbra has a larger inclination angle with respect to the surface normal than the bright component, everywhere in the penumbra. The maximum inclination difference is 8°. In the inner and mid penumbra, bright features (penumbral grains) are associated with an upflow of about $0.6\,\mathrm{km\,s^{-1}}$. At the outer spot boundary, the flow is inclined downwards predominantly in the dark component (-7°).

Key words: Sun: photosphere – Sun: sunspots – Sun: magnetic fields

1. Introduction

Important physical processes in sunspots occur on very small spatial scales, at or below the resolution limit of the instruments that are currently available. In the past, there have been conflicting results concerning a relationship between the magnetic field strength, the material flow and the brightness of the narrow, elongated penumbral filaments (see review of Wiehr 1999). Some observers reported a correlation between the intensity and the magnetic field strength, whereas Schmidt el al. (1992) found a correlation between the magnetic field inclination and the intensity, and no variation of the field strength. From a statistical analysis of two-dimensional data, Title et al. (1993) find a correlation between brightness and the velocity of the Evershed flow, and a difference of some 5° between the inclination angle of the bright and dark component.

From the analysis of one-dimensional slit spectra, observers could not establish a clear relationship between brightness and inclination angle, of either the material flow or the magnetic field. This has often been correctly addressed to insufficient spatial resolution. On the other hand, slit spectra always intersect the penumbra at different spot radii, thus mixing the properties of inner, central and outer penumbra.

Neglecting the small-scale structure, Schlichenmaier & Schmidt (2000, hereafter referred to as SS2000) have described the overall geometry of the Evershed flow in the deepest observable layers of a sunspot penumbra. They find an upflow in the inner part of the penumbra, followed by nearly horizontal motion in the middle penumbra. At the outer edge of the spot, but still inside the spot, the flow is slightly inclined downwards.

In the present work we apply a refined analysis to the same data, which allows us to distinguish between the material flow in the bright and the dark penumbral elements. We compare our findings with the predictions of the moving tube model (Schlichenmaier et al. 1998): This model describes the penumbral filaments as magnetic flux tubes in which hot material is moving upwards and outwards due to an internal gas pressure gradient. In the outflow phase the material cools by radiation. Therefore a penumbral filament that appears bright in the inner penumbra may become dark towards the outer penumbra.

2. Observations and data reduction

The observations have been carried out at the German Vacuum Tower Telescope in the Observatorio del Teide, Tenerife, from 8 to 11 November 1998. We used the filter spectrometer TESOS (Kentischer et al. 1998) to take two-dimensional spectra of a sunspot and its immediate surroundings. The Doppler velocity has been derived from the Fe II line at 542.5 nm, which is formed in the deep photosphere, at an optical depth $\tau_{500} = 0.1$. For the velocity measurements we used a Fourier phase method: The phase of the first Fourier component of the line profile provides the wavelength position (c.f., SS2000). At a spatial resolution of some 500 km, we have observed an isolated round sunspot (NOAA 8578). In the present analysis we concentrate on the data set, taken at a position angle of 11°. The observations and the properties of the spectral line used are described in more detail in SS2000.

2.1. Selection of bright and dark component

The intensity distribution in the penumbra is rather broad (e.g., Grossmann-Doerth & Schmidt 1981) and the mean intensity also depends on the spot radius. Therefore, a local definition of "bright" and "dark" has to be made. To this end, we converted the intensity data to polar coordinates relative to the spot center, and applied an azimuthal boxcar smoothing (box size ≈ 3.6

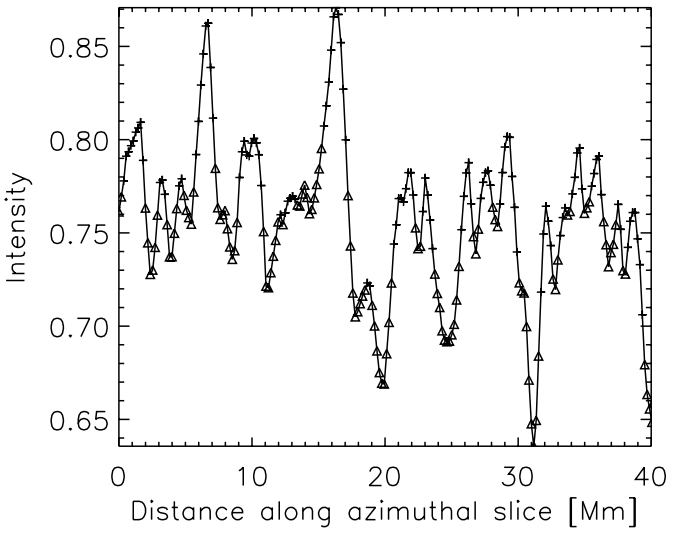

Fig. 1. Penumbral intensity (normalized to quiet Sun) at a fixed spot radius (10.3 Mm) versus azimuthal distance. Bright features are marked with a plus sign and dark features with a triangle. For better visibility, only the first 40 Mm of the azimuthal slice is plotted.

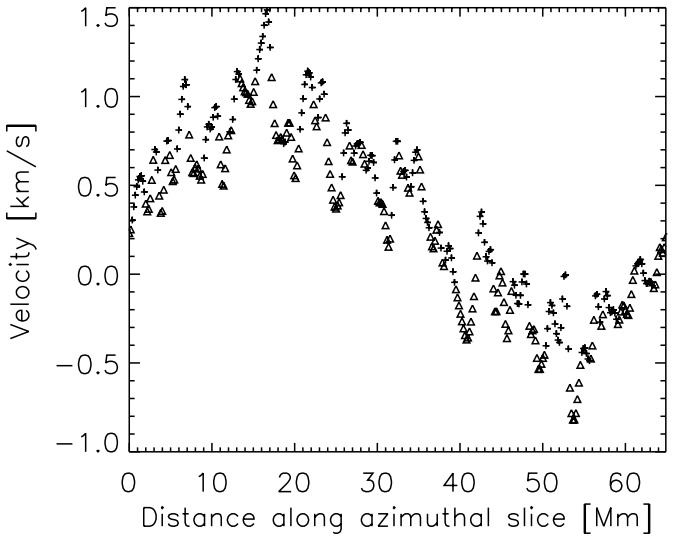

Fig. 2. Velocities at the locations of bright and dark pixels along the same azimuthal slice as in Fig. 1, except that entire slice is plotted.

Mm) to the continuum intensity values. For each radius, values above the mean were defined as "bright", and vice versa. With this definition, about half of the pixels are bright, and the other half are dark (50.5%, 49.5%). An example of that procedure is shown in Fig. 1. The graph contains part of an azimuthal slice of the continuum intensity at a spot radius of 10.3 Mm (inner penumbra). A boxcar average (not shown in the figure) has been applied to distinguish locally between bright and dark features. The plusses denote the bright component and the triangles correspond to the dark one. At the smallest spatial scale there are some very weak local darkenings that are not recognized as "dark" filaments, but the vast majority of (locally) dark and bright structures is correctly identified. White light images and filtergrams (being recorded simultaneously by TESOS) were co-aligned to find the co-spatial information within the velocity maps. The velocities corresponding to bright and dark pixels are plotted in Fig. 2 for the same spot radius as in Fig. 1. Here, the entire azimuthal slice is displayed, to demonstrate the sinusoidal modulation of the LOS-velocity in azimuth. Note that in most cases, the velocities corresponding to the bright (dark) features are above (below) the local mean.

2.2. Flow angle and flow velocity

We take advantage of the azimuthal variation of the line-of-sight velocity in order to determine the mean flow vector. In this paper we perform the analysis not only for the mean flow (as in SS2000), but also for the flow of the bright and dark component, separately. Neglecting an azimuthal component of the penumbral flow field, the line-of-sight measurement, $v^{\rm LOS}$, is related to the material flow on the Sun through

$$v^{\rm LOS}(r,\phi) = v_0(r,\phi) \cdot [\sin\theta\cdot\sin\phi\cdot\sin\gamma(r,\phi) + \cos\theta\cdot\cos\gamma(r,\phi)], \quad (1)$$

where v_0 is the flow velocity, θ is the heliocentric angle of the sunspot, γ denotes the inclination angle of the flow with respect to the surface normal and ϕ is the azimuth angle of the sunspot, with $\phi = 90^\circ$ pointing to disk center. Since the deviation of the penumbral flow field from axisymmetry is small, we describe the flow vector by azimuthal means.

From the measurements, $v^{\rm LOS}(r,\phi)$, we extract the vertical and horizontal components of the line-of-sight velocity. The vertical contribution to the line-of-sight velocity is given by its azimuthal mean, $m(r) := \langle v^{\rm LOS}(r,\phi)\rangle_\phi$,

$$v_\perp^{\rm LOS}(r) = \langle v^{\rm LOS}(r,\phi)\rangle_\phi = v_0(r)\cos\theta\cos\gamma(r) =: m(r), \quad (2)$$

and the horizontal contribution is described by

$$v_\parallel^{\rm LOS}(r,\phi) \;=\; v_0(r)\sin\theta\sin\gamma(r)\cdot\sin\phi =: A(r)\cdot\sin\phi, \quad (3)$$

A(r) is the amplitude of the azimuthal sinusoidal variation. The mean, m, and the amplitude, A, are obtained by fitting the function $f(m,A,\phi) = m + A\cdot\sin\phi$ to the measured velocities along an azimuthal slice, taking into account the uncertainty $\sigma(\phi)$ (see Sect. 2.3). The fit procedure is performed by minimizing

$$\chi^2(m,A) = \sum_{i=1}^{N}\left[\frac{1}{\sigma(\phi_i)}(v^{\rm LOS}(\phi_i) - f(m,A,\phi_i))\right]^2, \quad (4)$$

using the Marquardt algorithm (e.g., Bevington & Robinson 1992). The inclination angle, $\gamma(r)$, is computed from Eqs. (2) and (3) as

$$\gamma(r) = \arctan\left(\frac{A(r)}{m(r)\cdot\tan\theta}\right) \quad . \quad (5)$$

The absolute flow velocity, $v_0(r)$, is given as

$$v_0(r) = \frac{m(r)}{\cos\theta\cdot\cos\gamma(r)} = \frac{A(r)}{\sin\theta\cdot\sin\gamma(r)} \quad . \quad (6)$$

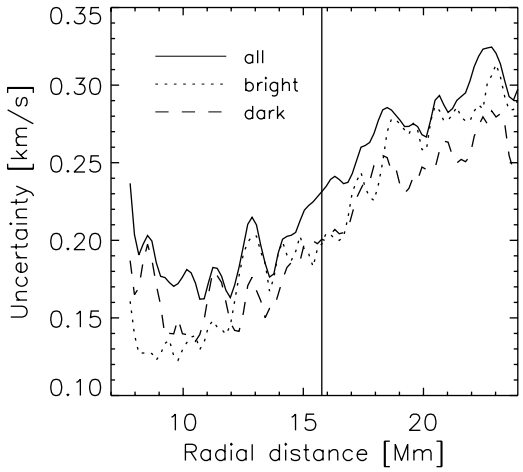

Fig. 3. The standard deviation of the measured velocity fluctuations along azimuthal slices versus radial distance from spot center. The penumbra spans from the left end of the abscissa to the vertical line at some 16 Mm. The fluctuations mainly stem from the fine structure of penumbra and granulation.

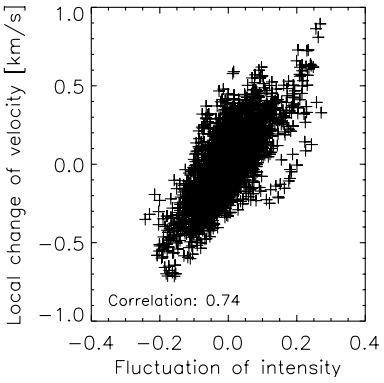

Fig. 4. Scatter plot of velocity versus brightness fluctuations in the center side ($20^\circ < \phi < 160^\circ$) of the inner penumbra ($6.5\ \mathrm{Mm} < r < 11.1\ \mathrm{Mm}$, corresponding to the range of the dotted line in Fig. 5) for $\theta = 11^\circ$. The velocity fluctuations are defined as the deviations from a boxcar-smoothed local mean in km s^{-1}, and the intensity fluctuations are given relative to the azimuthal mean of a specific slice.

2.3. Error analysis

Several sources of error have to be considered for the determination of m and A (cf. Eq. (4)): Measuring the LOS velocity is spuriously affected by seeing variations while scanning the line profile (see SS2000) and by determination of the line position. The largest uncertainty, however, is introduced by the penumbral fine structure itself: The velocity vectors of the bright and dark components differ significantly. This introduces a deviation from axisymmetry, i.e. from a sinusoidal shape of azimuthal velocity slices. The root-mean-square values of these small-scale deviations can be used as a measure of the uncertainty σ in Eq. (4).

Fig. 3 shows the radial dependence of σ for all pixels (solid line), for the bright (dotted line) and for the dark component (dashed line). In comparison with Fig. 2, it is seen that the rms values within the penumbra are small compared to the amplitude of the azimuthal variation of the velocity. Note that for all radii, the rms of the velocity fluctuation is smaller in the individual components (bright and dark) than for all data points. This indicates that the fit parameters m and A adopt different values for the bright and dark component.

The standard deviations of the fit parameters, σ_A and σ_m, correspond to the diagonal of the error matrix, which is calculated by the Marquardt algorithm (cf. Eq. (4)). The uncertainties for the flow angle, σ_γ, and for the flow velocity, σ_{v_0}, result from analyzing the error propagation. In addition to σ_A and σ_m, one has to consider the error in the position angle, θ, which is taken from synoptic maps. We estimate this error to be $\sigma_\theta = 1^\circ \simeq 0.017$ rad and ignore the slight variation of θ across the spot. Using Eqs. (5) and (6), we obtain:

$$\sigma_\gamma^2 = \sigma_A^2 \left(\frac{\partial\gamma}{\partial A}\right)^2 + \sigma_m^2 \left(\frac{\partial\gamma}{\partial m}\right)^2 + \sigma_\theta^2 \left(\frac{\partial\gamma}{\partial\theta}\right)^2$$

$$= \frac{\sigma_A^2 m^2 + \sigma_m^2 A^2 + \sigma_\theta^2 \cdot \frac{4A^2m^2}{\sin^2(2\theta)}}{\left[m^2\tan\theta + \left(\frac{A^2}{\tan\theta}\right)\right]^2} \qquad (7)$$

and

$$\sigma_{v_0}^2 = \sigma_A^2 \left(\frac{\partial v_0}{\partial A}\right)^2 + \sigma_m^2 \left(\frac{\partial v_0}{\partial\gamma}\right)^2 + \sigma_\theta^2 \left(\frac{\partial v_0}{\partial\theta}\right)^2$$

$$= \left[\frac{\sigma_A^2}{A^2} + \sigma_\gamma^2 \left(\frac{\cos\gamma}{\sin\gamma}\right)^2 + \sigma_\theta^2 \left(\frac{\cos\theta}{\sin\theta}\right)^2\right] \cdot v_0^2 \ . \qquad (8)$$

3. Results

In this paper we present the results obtained from our best data set at $\theta = 11^\circ$. We have carried out the same analysis for various position angles of the same spot (i.e. different observing days) and find consistent results (see also SS2000).

A systematic difference between the velocity field of the bright and dark component is apparent in Fig. 2. In order to elaborate on this impression quantitatively, we investigate the relation between the intensity of the penumbral filaments and the velocity pattern. A simple correlation analysis between the intensities and velocities comprising the whole penumbra would not provide useful information, since the measured flow depends both on radius and on azimuth. Thus we correlated the fluctuations of the velocity and intensity: In order to filter out the sinusoidal variation of the velocity signal, the velocity fluctuations are defined as the deviations from a local mean, which is obtained by a boxcar average with a width of $\Delta\phi = 45^\circ$ in azimuth. The intensity fluctuations are determined relative to the azimuthal mean for each radial position: $(I(r,\phi) - \langle I(r,\phi)\rangle_\phi)/\langle I(r,\phi)\rangle_\phi$. The intensity values were taken from the best continuum image recorded together with the co-spatial spectra, i.e. the intensity and velocity values are simultaneous, but independent, measurements. In Fig. 4 we show the correlation between the velocity fluctuation and the inten-

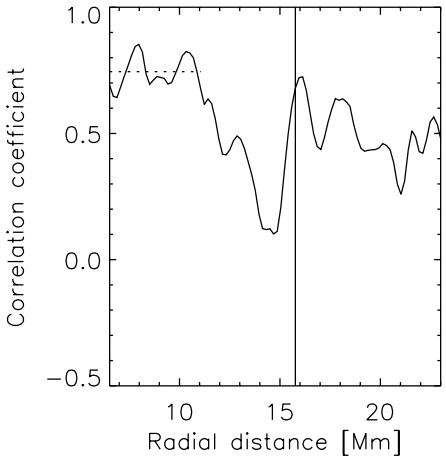

Fig. 5. Correlation coefficient of azimuthal slice between velocity and brightness fluctuations as a function of spot radius. As in the previous figure, only a central sector of $140°$ is considered. The penumbra spans from the left end of the abscissa to the vertical line.

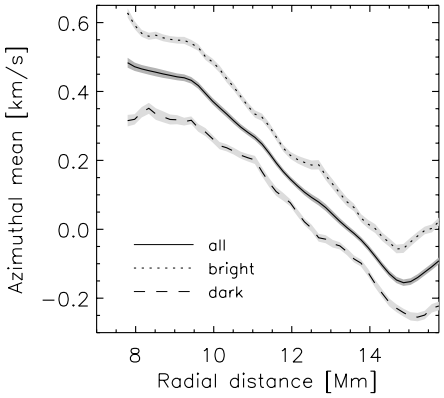

Fig. 6. Azimuthal mean, $m(r)$, of the penumbral velocity as a function of spot radius for $\theta = 11°$. Dotted line: bright points; dashed line: dark points; full line: all data. The shaded areas are the 1σ error bars.

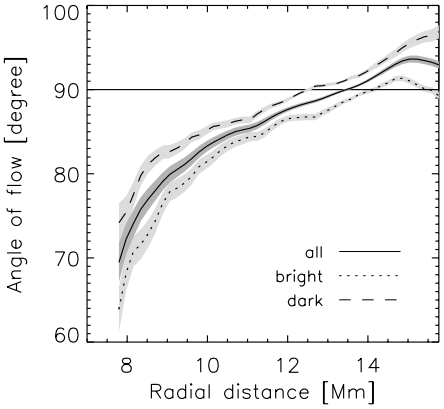

Fig. 7. Inclination angle, $\gamma(r)$, of the penumbral flow. As Fig. 6.

sity variation for the inner penumbra of the center-side of the spot. The azimuth angle, ϕ, ranges from $20°$ to $160°$. The inner penumbra comprises pixels with a spot radius, r, between 6.5 Mm and 11.1 Mm (corresponding to the range of the dotted line in Fig. 5). Positive velocity is clearly correlated with brightness, i.e. the strongest upflows occur in the brightest parts. This has already been reported by Schlichenmaier & Schmidt (1999). In the outer parts of the penumbra the correlation disappears, as can been seen in Fig. 5. This is not surprising, since the flow is mostly horizontal and occurs both in dark and bright filaments.

As a next step, we divided the observed line-of-sight velocity maps in a "bright" and a "dark" component, using the local intensity criterion described above. Using Eqs. (4) – (6), we derived the inclination angle, the azimuthal mean velocity, and the magnitude of the flow for each of the ensembles (all, bright, and dark) separately.

The azimuthal mean, the inclination angle and the absolute flow velocity for the data set with $\theta = 11°$ are shown in Figs. 6 to 8. Fig. 9 displays the inclination angle for our data set at $\theta = 20°$. The azimuthal mean $m(r)$, i.e. the vertical velocity component, of the bright component is larger than $m(r)$ in the dark component everywhere in the penumbra. Both components decrease with radial distance. We find that the flow angle (Fig. 7) of the bright component is always less inclined with respect to the surface normal than the dark component. In the inner penumbra, the flow in the bright component is more vertically oriented (due to a larger vertical velocity) than the flow in the dark one. Since the seeing conditions were somewhat worse for our data set at $\theta = 20°$, the absolute difference between the bright and dark component is smaller. The flow in the dark component bends downwards ($\gamma > 90°$) already at a about two thirds of the penumbral width ($r \approx 12.5$ Mm) to reach a downflow angle of $7°$ ($\gamma = 97°$) at the outer penumbral edge (due to a negative vertical velocity), whereas the bright component never shows a significant downflow. The maximum inclination difference between dark and bright is about $8°$.

The shaded areas surrounding each plotted line mark the 1σ error bars, as obtained from the analysis of Sect. 2.3. These error bars demonstrate that the results concerning the azimuthal mean and the inclination angle (Figs. 6 and 7) are significant everywhere in the penumbra. The errors are significantly larger for the absolute flow velocity (Fig. 8): the flow speed of the bright component lies within the 1σ error bars of the dark component, and vice versa. Since the flow is predominantly horizontal, the main source of this error is the uncertainty of the position angle, θ. Near disk center, i.e. for small θ, only a small fraction of the horizontal velocity component is measured. From Eq. (8) we see that any error in θ is amplified by $\approx 1/\tilde{\theta}$, where $\tilde{\theta}$ is the position angle in radian. Indeed, for larger θ, the 1σ error becomes smaller, as is seen in Figs. 10 and 11, which display the dependence of the flow velocity for $\theta = 20°$ and $\theta = 25°$, respectively. In these figures, the dark component shows a significantly larger velocity in the outer penumbra than the bright component. This indicates that the flow field of the outer penumbra is dominated by the dark component.

4. Discussion

The penumbral flow field is predominantly horizontal, but a vertical component is present which decreases with radial distance

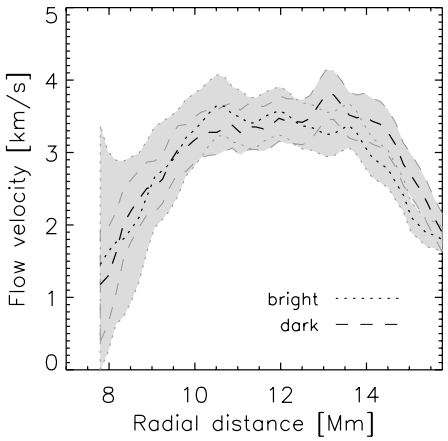

Fig. 8. Penumbral flow speed, v_0, for $\theta = 11°$. As Fig. 6, except that only the bright and dark component is plotted. To distinguish between the overlapping error bars, each of the two areas is surrounded by gray lines (dotted for bright points and dashed for dark points).

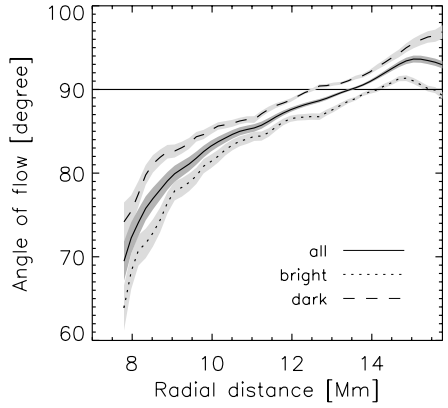

Fig. 9. As Fig. 7, but for $\theta = 20°$.

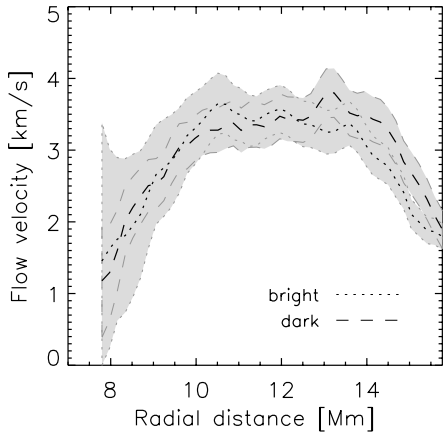

Fig. 10. Same as Fig. 8, but for $\theta = 20°$. The 1σ error bars of the bright and dark component do not overlap in the outer penumbra.

from spot center. This leads to an upflow component in the inner part of the penumbra, which gradually changes into a downflow component in the outer penumbra. In the previous section we

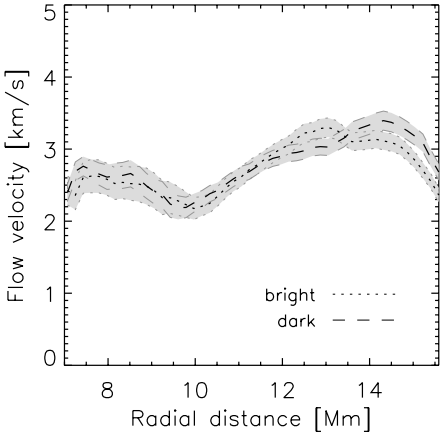

Fig. 11. Same as Figs. 8 and 10, but for $\theta = 25°$.

presented significant differences in the material flow geometry for bright and dark penumbral features.

The bright component of the flow is less inclined with respect to the surface normal than the dark component throughout the entire penumbra. In the inner penumbra, bright features correspond to patches of upflows, whereas dark features are in average more horizontal. This indicates that bright penumbral features, i.e. penumbral grains and bright filaments, are consistent with the moving tube model (Schlichenmaier et al. 1998) which suggests that hot sub-photospheric plasma is transported by upflow channels into the penumbral photosphere. We have estimated that these upflows are sufficient to explain the surplus brightness of the penumbra relative to the umbra (Schlichenmaier & Schmidt 1999).

In the outer part of the penumbra only the dark component shows a downflow. The flow speed in the dark component is somewhat higher than in the bright features. Assuming that the flow channels are confined by magnetic flux tubes, they may be advected by the flow field of the surrounding granulation into the cool intergranular lanes.

The spatial resolution of our data is about 500 km, just good enough to distinguish between two, locally defined, intensity ranges and to measure the material flow speed there. We expect that at higher resolution much higher flow speeds and larger velocity fluctuations would result.

The analysis of two-dimensional velocity data, covering the complete spot reveal some of the difficulties that arise when working with one-dimensional spectra taken with a grating spectrograph: the slit (assumed to be straight) always intersects the penumbra at different spot radii, and the data base from a single spectrum is too small to establish a relationship between intensity (or temperature) and other quantities, such as velocity and magnetic field.

Acknowledgements. Part of this work was supported by the *Deutsche Forschungsgemeinschaft, DFG*. We are indebted to M. Stix for valuable comments on the manuscript. We thank H. Peter and K. Hartkorn for sharing with us their knowledge on error analysis.

References

Bevington P.R., Robinson D.K., 1992, Data reduction and error analysis for the physical sciences. 2nd ed., McGraw–Hill
Grossmann-Doerth U., Schmidt W., 1981, A&A 95, 366
Kentischer T., Schmidt W., Sigwarth M., v. Uexküll M., 1998, A&A 340, 569
Schlichenmaier R., Schmidt W., 1999, A&A 349, L37
Schlichenmaier R., Schmidt W., 2000, A&A 358, 1122 (SS2000)
Schlichenmaier R., Jahn K., Schmidt H.U., 1998, A&A 337, 897
Schmidt W., Hofmann A., Balthasar H., Tarbell T.D., Frank Z.A., 1992, A&A 264, L27
Title A.M., Frank Z.A., Shine R.A., et al., 1993, ApJ 403, 780
Wiehr E., 1999, In: Schmieder B., Hofmann A., Staude J. (eds.) Third Advances in Solar Physics Euroconference: Magnetic Fields and Oscillations. ASP Conf. Ser. vol. 184, p. 86